

# Attractor selection based limited feedback hybrid precoding for uplink V2I communications

Junliang Ye, *Member, IEEE*, and Hamid Gharavi, *Life Fellow, IEEE*

National Institute of Standards and Technology (NIST)

Gaithersburg, MD 20899, USA

Emails: junliang.ye@nist.gov, hamid.gharavi@nist.gov

**Abstract**—As an essential part of vehicle networks, the Vehicle to Infrastructure (V2I) needs the support of millimeter wave and massive MIMO technologies to enable high data rate applications, such as automated driving, real-time high-quality multimedia services and so on. As the scale of the antenna array increases, the complexity of the beamforming and channel estimation algorithms under high mobility conditions also increases significantly. In particular, highly robust beamforming methods need to cope with fast changing transmission environments. In this paper, we adopt a biological inspired self-adaptive selection algorithm called attractor selection algorithm (ASA) to support uplink beamforming. The ASA requires only a little feedback information from the Road Side Infrastructure (RSI) to perform fast beam training, hence making the transmission link more stable. The simulation results indicate that the proposed ASA-assisted algorithm can significantly reduce the time required to achieve a timely beam training, which would be essential for V2I high communications under high mobility conditions.

## I. INTRODUCTION

Millimeter wave (mmWave) communications and massive multiple input multiple output (massive MIMO) are two key technologies that are capable of supporting the extreme performance requirements of the 5th generation cellular network (5G) systems [1]. Compared to sub-6 GHz transmissions, the use of massive MIMO technology can effectively overcome the high path loss of mmWave transmissions [2]. In addition, mmWave with a large number of antenna arrays, offers significant benefits in terms of transmission rate and delay [3], which makes it highly suitable for vehicle networking [4], [5]. However, due to wide ranging vehicle velocities for V2I communications, the transmission environment of vehicular communications is more complex than regular cellular communications [6]. For instance, to overcome the path loss of mmWave signals, the beamwidth should be as narrow as possible and this can only be accomplished with the help of massive MIMO technology [7]. For V2I uplinks in particular the main challenge is how to perform fast beamforming, especially at high velocities [8]. In addition, to achieve very narrow beamforming, large scale antenna arrays would be essential and this can further add to the complexity of the precoding method [9]. Thus,

compared with sub-6 GHz based regular uplink beamforming methods, that are used in cellular networks, mmWave based uplink beamforming requires greater computational time for beam training or RSI switching.

Beamforming of vehicular communication, based on mmWave and massive MIMO technology has become a hot topic in recent years. Most previous works mainly concentrated on hybrid precoding and developing methods to reduce hardware complexity [10]–[16]. For instance, the massive MIMO systems are studied in [17]–[19] to support high data rate wireless communications. For stationary/low-velocity mmWave communication systems with large antenna arrays, the authors of [19] show the impact of the optimal beamforming design in attaining a good performance. Beam management and multiple beam training methods are comprehensively covered in [20]. To analyze the coverage of urban mmWave microcellular networks, [21] investigates a stochastic geometry based theoretical model, which proposes a tractable framework to characterize the downlink coverage performance of urban mmWave. The authors in [22] introduce a theoretical model to characterize the link budget requirements of mmWave networks to provide downlink connectivity to highway vehicular networks. They also discuss the relationship between beamwidth and signal to interference, plus noise ratio (SINR). Due to narrower beamwidths (compared with sub-6GHz transmissions), mmWave based beamforming technologies have been frequently investigated with the aid of positioning systems. For example, applications and challenges of mmWave based positioning, as well as comparison between different positioning technologies, have been studied in [23]. Mmwave based beamforming technology can greatly benefit from more frequent beam alignment and signal training. A novel beam alignment method using multipath fingerprints positioning technology is proposed in [24] where the positioning information is used to enhance the efficiency of precoding algorithms. To accelerate information propagation along the highway, In [25], a virtual-MIMO-enabled information dissemination scheme was investigated to enable vehicles to form virtual antenna arrays opportunistically in order to boost the transmission range.

All the above beamforming methods require either: a complex channel estimation or additional data, such as positioning information. Under high vehicular velocity conditions, however, channel information-based beamforming methods may not always be practical due to computational complexity [26]. On the other hand, there are other studies that focus on less complex codebook-based beamforming methods. In [27] a Lloyd-type algorithm is proposed to construct a codebook to assist hybrid beamforming in a frequency selective mmWave transmission environment. In order to reduce the complexity of hybrid precoding, the authors of [28] present a hierarchical search scheme, which uses a pre-designed analog hierarchical codebook to search multiple beams. Considering the practical limitations of phase shifters, [29] proposes a codebook-based RF precoder to develop joint optimization of RF-baseband precoders in multiuser mmWave systems. Similarly, in [30] a codebook for analog beam steering with quantized phase shifters is designed in order to improve performance in terms of average achievable spectral efficiency and lower hardware cost. The optimization of an analog codebook is investigated in [31], which aims to approximate a fully-digital codebook by means of a hybrid architecture requiring only 2-bit RF phase shifters.

By using codebook for the analog beamforming, the complexity of hybrid beamforming can be significantly reduced. However, all the aforementioned studies did not offer a method for beam pattern selection under a highly dynamic communication scenario. While these studies aim at reducing the complexity of codebook-based hybrid precoding, there are a few investigations that focus mainly on selecting the best beam pattern from the codebook in order to enhance robustness and stability [32]–[34]. In particular, a bio-inspired algorithm, such as ASA has been receiving considerable attention due to its self-adaptivity and robustness in highly dynamic environments. ASA was initially proposed in [35] to provide a mechanism of cell selection dominant gene expression in a limited feedback environment. Subsequently, it was adopted to solve the routing problem in Ad hoc networks [36]. ASA can also be used in heterogeneous vehicular networks to deal with network selection problems [37] [38]. More studies of ASA applications in wireless networks can be found in [39].

In this paper, we adopt ASA to support uplink beamforming in V2I communication scenario to overcome the instability caused by vehicles moving at series velocities. The contributions of this paper are summarized as follows;

- 1) We propose an ASA-assisted uplink beam training method capable of achieving fast beamforming in V2I communications. A unique feature of the proposed beam training method is that it only needs limited feedback from RSIs, hence significantly reducing the complexity of beamforming algorithms.

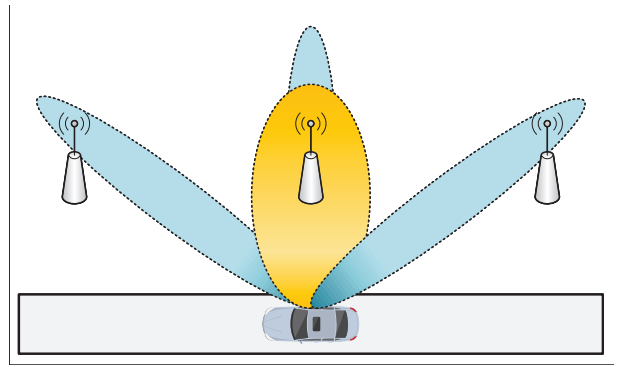


Fig. 1. Uplink beamforming of V2I communications.

- 2) We develop an ASA-assisted multiresolution codebook where a transmitter can adaptively adjust its beamwidth to cope with varying channel conditions caused by the high-speed mobility of vehicles. The simulation results indicate that the proposed method can effectively reduce the time required for beam training. The simulation results also indicate that the proposed ASA-assisted beamforming method does not require densely deployed RSIs to achieve a good performance.
- 3) ASA functionality depends on several parameters and each has a significant influence on the efficiency of the algorithm. An important aspect of our proposed method is the proper configurations of these parameters that can lead to a considerable performance improvement of the ASA-assisted beamforming algorithm.

The rest of the paper is organized as follows: The system model and ASA algorithm are described in section II. Section III introduces a multiresolution codebook based mmWave precoding design, including the derivation process of parameters in ASA. Simulations of the proposed algorithm are carried out in section IV. Conclusions are finally drawn in section V.

## II. SYSTEM MODEL

The system model is based on a scenario where a vehicle is moving on a road in an urban or suburban area as shown in Fig.1. In this scenario, we assume that there are roadside infrastructure (RSI) units situated along the road. Their number and locations are assumed to be governed by a one dimensional homogeneous Poisson point process (PPP) with intensity,  $\lambda_{RSI}$ . Without loss of generality, the movements of vehicles are assumed to be restricted to one lane (e.g., the vehicles are not able to change lanes). Furthermore, the velocity of the moving vehicle is assumed to be governed by a Gauss-Markov mobility model, which has been widely used for the modelling of one dimensional

or two dimensional movements. Based on [40], the velocity of the vehicle can be expressed as,

$$v_m(t + \Delta t) = \delta_r v_m(t) + (1 - \delta_r) \bar{v}_m + \sqrt{1 - \delta_r^2} \mathcal{N}_{GM} \quad (1)$$

where  $v_m(t)$  is the moving velocity of a vehicle at time  $t$ ,  $\bar{v}_m$  represents the average moving velocity of all vehicles in the same lane,  $\mathcal{N}_{GM}$  is a Gaussian distributed random variable with expectation  $\mu_{GM}$ , and  $0 \leq \delta_r \leq 1$  is a parameter that reflects the degree of randomness, e. g.,  $\delta_r = 0$  and  $\delta_r = 1$  indicates the lowest and highest degree of randomness, respectively. Moreover, the Gauss-Markov mobility model expressed in (1) can be represented in discrete form as,

$$v_m(k_t + 1) = \delta_r v_m(k_t) + (1 - \delta_r) \bar{v}_m + \sqrt{1 - \delta_r^2} \mathcal{N}_{GM} \quad (2)$$

where  $v_m(k_t)$  is the vehicle velocity at given time slot  $k_t$ .

We consider mmWave and massive MIMO using a hybrid precoding technology for uplink communications between vehicles and RSIs. According to [20], the initial access phase should be done before data transmission. For the sake of further analysis, we assume that the initial access phase starts at the beginning of each time interval. More specifically, uplink transmissions in the initial access phase will be searched in a sectorized scanning manner using omnidirectional or quasi-omnidirectional antennas by each RSI. A vehicle will then establish an association with a specific RSI upon receiving an uplink transmission request by the vehicle in the initial access phase. Then, the beamforming pattern of the vehicle will be adjusted by using feedback information from the RSI to enhance the performance of the uplink transmission.

#### A. Attractor selection algorithm

Attractor selection algorithm (ASA) is a biologically inspired method for self-adaptively selecting one of several candidates which best reflects the current situation in a highly dynamic environment. In [35], the authors propose ASA for capturing the synthetic bi-stability in the situation where the gene expression is governed by two mutually inhibitory operons. This original ASA is represented by a nonlinear stochastic dynamical system consisting of two ordinary differential equations,

$$\begin{cases} \frac{dm_1}{dt} = \frac{S(A)}{1+m_1^2} - D(A) \times m_1 + \eta_1 \\ \frac{dm_2}{dt} = \frac{S(A)}{1+m_2^2} - D(A) \times m_2 + \eta_2 \end{cases} \quad (3)$$

$$\begin{cases} S(A) = \frac{6A}{2+A} \\ D(A) = A \end{cases} \quad (4)$$

In the above,  $m_1$  and  $m_2$  are the concentrations of the mRNAs or their protein products, transcribed from Operon1 and Operon2, respectively.  $S(A)$  and  $D(A)$  are the rate coefficients of synthesis and degradation/dilution due to cell

volume growth, respectively. Importantly, they depend on  $A$ , which represents cellular activity.  $\eta_1$  and  $\eta_2$  corresponds to independent white noise in gene expression. In this model, when the cell activity is high, the values of  $S(A)$  and  $D(A)$  will be large enough to ignore the effect of the noise term;  $\eta_1$  and  $\eta_2$ . So the values of  $m_1$  and  $m_2$  will become larger to fit the high cell activity based on (3). On the other hand, if the cell activity is low, the noise term  $\eta_1$  and  $\eta_2$  will strongly affect the value of  $m_1$  and  $m_2$  and force the cell to search for a new attractor to rebuild the balance between cell activity and the transcription of mRNAs.

As the vehicles are moving with a high velocity, the quality of the links between vehicles and RSIs becomes highly fluctuant and hard to be predicted, e. g., the quality of the links may change dramatically and stochastically due to movements of vehicles. Thus, by denoting the link quality as the cell activity and the beamforming pattern as the concentrations of the mRNAs, we can use the ASA to support the uplink beamforming process to enhance the robustness and stability of V2I communications. Here, we map the quality of the uplink to  $\alpha$ , which is shown in (3) as  $A$ . When the vehicle is moving, the value of  $\alpha$  will be fluctuant and hard to predict. Based on (3), if a proper uplink beamforming pattern is selected, i. e., a correct attractor ( $m_1$  or  $m_2$ ) that represents the environment is selected, the value of  $\alpha$  will become larger. Then, the uplink beamforming process, which is driven by ASA, will maintain this beamforming pattern until the value of  $\alpha$  becomes smaller again due to the mobility of the vehicle. Further details about how we map the link performance to parameters of ASA can be found in section II-B.

#### B. ASA-assisted limited feedback uplink beamforming

The channel condition is highly fluctuant for uplink vehicle communication due to the transmitters high velocity. The ASA can be used to make the link between RSIs and vehicles more stable for uplink beamforming. Furthermore, compared with general channel estimation-based uplink beamforming methods, the ASA-assisted uplink beamforming only requires limited feedback information of the link performance, which is very easily to achieve at the receiver side, e. g., the RSI. To achieve this, we first need to address the following two issues;

- 1) ASA can only be used to solve selecting issues. Bear in mind that widely used hybrid beamforming methods are mostly reliant on the accuracy of highly complex channel estimations where channel information from receivers is used to further optimize the performance of the link. However, since there is no selection process, the ASA cannot be applied here.
- 2) The original ASA has only two Operons as candidates. To adapt to varying environmental conditions

caused by wide ranging velocities, more candidates beamforming patterns are needed to achieve efficient beamforming for V2I communications.

Here, we first extend the original ASA to a multi operons case. To achieve this, we develop a codebook-based uplink beamforming method where each codeword in the codebook is assigned to a different operon.

The proposed extended ASA consists of  $M_{co}$  Operons where each corresponds to a beamforming pattern having a different direction and beamwidth. To reduce the time cost on beam training, the ASA can self-adaptively select the best uplink hybrid beamforming candidate based on the optimization of the following objective function  $\theta_{obj}$ ,

$$\theta_{obj} = (\beta_{ca}p_{ca} + \beta_{st}p_{st})p_{in} \quad , \quad (5)$$

where  $p_{ca}$  is the spectral efficiency of the corresponding beamforming pattern  $i$ ,  $p_{st}$  is the predicted duration that the associated RSI can stay in the main lobe of the current beam pattern,  $\beta_{ca}$  and  $\beta_{st}$  are the weight coefficients of  $p_{ca}$  and  $p_{st}$ , respectively.  $p_{in}$  is the indicator function, which is defined as,

$$p_{in} = \begin{cases} 1 & \text{if } \phi_{as} \in \mathbb{A}_{cur} \\ 0 & \text{if } \phi_{as} \notin \mathbb{A}_{cur} \end{cases} \quad , \quad (6)$$

where,  $\mathbb{A}_{cur}$  is the coverage area of the currently selected beamforming pattern and  $\phi_{as}$  is the location of the associated RSI of the corresponding vehicle.

Now, let us consider a set  $A_n = \{m_i | i = 1, 2, \dots, M_{co}\}$ , where  $m_i$  represents a selection weight of beamforming pattern  $i$ . Then, the probability of selecting pattern  $i$  to do the uplink beamforming is defined as,

$$P_i = m_i / \sum_{k=1}^{M_{co}} m_k \quad . \quad (7)$$

The dynamic behavior of  $m_i$  is characterized by the stochastic differential equation system given in (8) for  $i \in [1, 2, \dots, M_{co}]$ ,

$$\frac{dm_i}{dt} = \frac{syn(\alpha)}{1 + m_{cur} - m_i} - deg(\alpha) \times m_i + \eta_i \quad , \quad (8)$$

where  $m_{cur}$  is set as the current beamforming pattern before the beam training phase. The functions  $syn(\alpha)$  and  $deg(\alpha)$  are rate coefficients of mRNA synthesis and degradation in the original biological model, respectively. Both are monotonically increasing functions of  $\alpha$ , which represents cell activity or vigor and  $\eta_i$  corresponds to an independent white Gaussian noise component inherent in gene expression. Let us define  $syn(\alpha)$  and  $deg(\alpha)$  as [38],

$$syn(\alpha) = v_s \alpha^{k_s} + \alpha \quad , \quad (9)$$

$$deg(\alpha) = \alpha \quad . \quad (10)$$

The mechanism of ASA is explained as follows. Let us first consider a case in which an environmental change causes a notable decrease in  $\alpha$  due to the inappropriate (i.e., the cell is in the non-adaptive attractor) gene expression pattern. Then, the deterministic metabolic rate in (8) will be so small that it will approach the same magnitude as that of the noise term  $\eta_i$ . The dynamics of gene expression will, therefore, be dominated mostly by random fluctuations. This is true as long as the network is in a region with a state of low activity. On the other hand, when the network moves into a high activity region,  $\alpha$ , i.e., to the adaptive attractor, then the metabolic rate increases and the deterministic part becomes much larger than the noise term. Consequently, the dynamics of the system will be governed by the deterministic part of (8). Thus, regardless of the initial state of gene-expression of the network, it will continue to fluctuate until it arrives at the adaptive attractor, which is more stable against the noise. This is mainly because of the relatively larger metabolic rate of the first and second terms in (8).

By considering the case that  $dm_i/dt = 0$ , and ignoring the effect of  $\eta_i$ , the differential equation (8) is further derived as follows,

$$0 = \frac{syn(\alpha)}{1 + m_{cur} - m_i} - deg(\alpha) \times m_i \quad . \quad (11)$$

Based on (11), we can get the balance solution of (8) as,

$$m_i = \begin{cases} \Phi(\alpha) & \text{if } i = Cur \\ \frac{1 + \Phi(\alpha) - \sqrt{(1 - \Phi(\alpha))^2}}{2} & \text{if } i \neq Cur \end{cases} \quad , \quad (12)$$

where  $\Phi(\alpha) = syn(\alpha) / deg(\alpha)$ ,  $Cur$  means the currently selected beamforming pattern. Based on (12), we can see that if  $\Phi(\alpha) \leq 1$  then all  $m_i$  will converge to  $\Phi(\alpha)$ . Thus, based on (7), the probability that  $m_i$  is selected to be the beamforming pattern after current beam training phase will be the same and equals  $1/M_{co}$  for all  $M_{co}$  candidates beamforming patterns. Otherwise, the  $m_{cur}$  will be much larger than the other  $m_i$ , i.e., it is more likely for the vehicle to maintain the current beamforming pattern instead of starting a new beam training phase and generating extra beam training cost.

As  $syn(\alpha)$ ,  $deg(\alpha)$  and  $\Phi(\alpha)$  are all monotonically increasing functions of  $\alpha$ , the larger value of  $\alpha$  indicates better link performance and thus higher probability to be selected as the beamforming pattern. On the other hand, if the value of  $\Phi(\alpha)$  is small, then the selecting probability ( $P_i$ ) for all candidates is the same, thus the vehicle will randomly choose a beamforming pattern during the beam training phase. If  $\alpha$  is still very small after the last selection among all beamforming patterns, the beam training phase will continue until a suitable beamforming pattern is selected and  $\alpha$  rises to an acceptable level. Bear in mind that the

activity value  $\alpha$  reflects the goodness of the current solution of ASA. Its desired behavior is summarized as follows:

If we have no information about which beamforming pattern to choose, selection should be performed uniformly among all  $M_{co}$  codewords in the codebook as candidates. Therefore, the vehicle should initialize  $\alpha = 0$  as this corresponds to the no preference case, and a small value of  $\alpha$  means that the current codeword is not suitable and a new codeword should be searched. Conversely, a larger value of  $\alpha$  means greater gaps in selecting probability between different candidates, i.e., the current codeword fits the communication environment very well and there is no need to search for a new codeword.

So, the construction of the expression of  $\alpha$  is the most important issue of the ASA-assisted self-adaptive selection method. With the objective function defined as (5), the  $\alpha$  is further designed as,

$$\alpha = \begin{cases} \frac{\gamma_a}{1 + \exp\left(1 - \frac{\theta_{obj}}{\theta_{max}}\right)} & \theta_{obj} \geq \theta_{thr} \\ \frac{1}{1 + \exp\left(1 - \frac{\theta_{obj}}{\theta_{max}}\right)} & 0 \leq \theta_{obj} < \theta_{thr} \end{cases}, \quad (13)$$

where  $\theta_{max}$  is the upper bound of  $\theta_{obj}$ ,  $\theta_{thr}$  is a given threshold of  $\theta_{obj}$  and  $\gamma_a$  is a constant parameter. Consequently,  $\alpha$  is designed as a piecewise function in order to enlarge the gaps in the value of  $\alpha$  between large  $\theta_{obj}$  and small  $\theta_{obj}$ , i.e., gaps between good and bad performances. Now, we define the value of the objective function of the current beamforming pattern as  $\theta_{obj}^{cur}$ . Due to the path loss,  $\theta_{obj}^{cur}$  will become smaller when the distance between a vehicle and the associated RSI gets longer due to movement of the vehicle. So, as soon as  $\theta_{obj}^{cur}$  falls below  $\theta_{thr}$ , the corresponding value of  $\alpha$  will decrease dramatically, hence forcing the vehicle to find a better beamforming pattern through ASA in order to increase the value of  $\alpha$ , i.e., the performance of the link.

### III. MULTI-RESOLUTION CODEBOOK BASED UPLINK HYBRID PRECODING

#### A. Construction of multi-resolution codebook

In this section, we will use the method in [41] to construct a multi-level hybrid beamforming codebook in order to support the proposed ASA-assisted uplink beamforming. By denoting  $N_A$  as the total number of beam patterns in a codebook, we divide the two dimensional plane into  $N_A$  separated angulars with the width of each angular equal to  $2\pi/N_A$ .

We assume that the codebook is constructed with  $S = \log_2 N_A$  levels, and each level has a different beamwidth. The  $s$ th level of the codebook contains  $k = (M)^{s-1}$  subsets, where  $M$  is the number of column vectors, i.e., codewords for uplink hybrid precoding. We denote  $\mathbf{F}_A^{\{s,k,m\}}$  and  $\mathbf{F}_D^{\{s,k,m\}}$  as the analog and baseband codewords on level  $s$  ( $1 \leq s \leq S$ ), subset  $k$  ( $1 \leq k \leq (M)^{s-1}$ ),

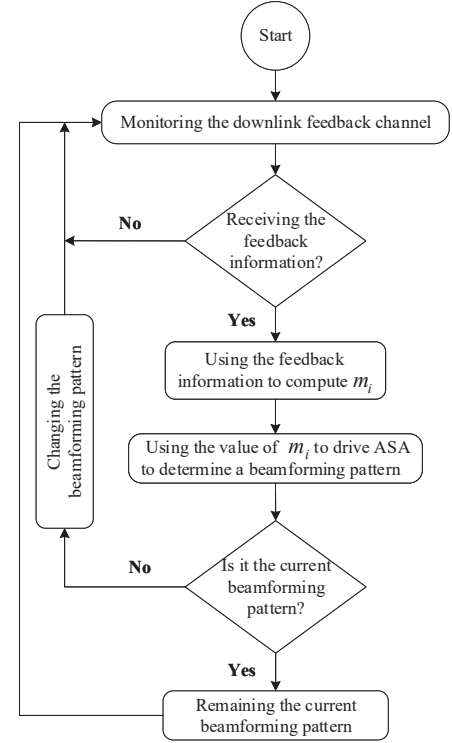


Fig. 2. The operating process of the ASA-assisted uplink beamforming.

and column  $m$  ( $1 \leq m \leq M$ ), respectively. Then, the corresponding hybrid precoding matrix is defined as  $\mathbf{F}_H^{\{s,k,m\}} = \mathbf{F}_A^{\{s,k,m\}} \mathbf{F}_D^{\{s,k,m\}}$ , and the range of angular of departure (AoD) of each level in the codebook  $\mathcal{F}$  is configured as in Fig. 3.

More details of construction process of the codewords can be found in the Appendix.

#### B. Codebook based limited feedback uplink hybrid precoding

Based on the analysis in [42], the geometrical channel model with  $L$  propagation paths is given as,

$$\mathbf{H} = \sqrt{N_T N_R} \sum_{l=1}^L \psi_l \mathbf{a}_R(\theta_l) \mathbf{a}_T(\varphi_l) \quad (14)$$

Where  $N_T$ ,  $N_R$ ,  $\psi_l$ ,  $\mathbf{a}_R(\theta_l)$ , and  $\mathbf{a}_T(\varphi_l)$  are the number of transmit antennas, the number of receive antennas, the channel gain of the  $l$ th propagation path, the array response of receive antenna array with angular of arrival (AOA) as  $\theta_l$ , and the transmit antenna array with AOD as  $\varphi_l$ , respectively. Formula (14) can be further expressed in matrix form as,

$$\mathbf{H} = \sqrt{N_T N_R} \mathbf{A}_R \boldsymbol{\Psi} \mathbf{A}_T, \quad (15)$$

with,

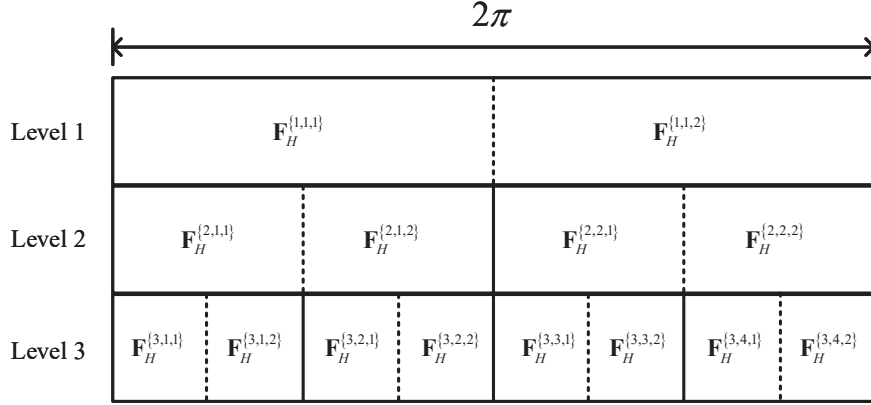


Fig. 3. An example of a three levels codebook with  $N_A = 8$  and  $M = 2$ .

$$\begin{aligned} \mathbf{A}_R &= [\mathbf{a}_R(\theta_1) \dots \mathbf{a}_R(\theta_L)] \\ \psi &= \text{diag}[\psi_1 \dots \psi_L] \\ \mathbf{A}_T &= [\mathbf{a}_T(\varphi_1) \dots \mathbf{a}_T(\varphi_L)] \end{aligned} \quad (16)$$

Where  $\text{diag}[\cdot]$  is a diagonal matrix with  $l$ th entry as  $\psi_l$ . Consider each vehicle is equipped with a uniform linear array, then the corresponding array response can be expressed as,

$$\mathbf{a}_R(\theta_l) = \frac{1}{\sqrt{N_R}} [1, e^{j\theta_l}, \dots, e^{j(n_R-1)\theta_l}] \quad , \quad (17)$$

and,

$$\mathbf{a}_T(\varphi_l) = \frac{1}{\sqrt{N_T}} [1, e^{j\varphi_l}, \dots, e^{j(n_T-1)\varphi_l}] \quad , \quad (18)$$

where  $j$  is the imaginary unit.

By denoting the analog precoder and digital precoder as  $\mathbf{F}_A \in \mathbb{C}^{N_T \times N_{RF}}$  and  $\mathbf{F}_D \in \mathbb{C}^{N_{RF} \times N_S}$ , the signal vector  $\mathbf{x}$  after analog and digital precoding is given by,

$$\mathbf{x} = \mathbf{F}_A \mathbf{F}_D \mathbf{z} \quad , \quad (19)$$

where  $\mathbf{z} \in \mathbb{C}^{N_S}$  denotes the information symbols from the  $N_S$  data streams and  $N_{RF}$  is the number of activated RF chains. Based on [42], given a certain analog precoder  $\mathbf{F}_A$ , the corresponding optimal digital precoder is expressed by,

$$\mathbf{F}_D = (\mathbf{F}_A^H \mathbf{F}_A)^{-1/2} \overline{\mathbf{V}} [1, \dots, s] \mathbf{\Lambda}^{1/2} \quad , \quad (20)$$

Since the optimal digital precoder is based on the water filling algorithm, for a large number of antennas (20) can be further approximated as,

$$\mathbf{F}_D = (\mathbf{F}_A^H \mathbf{F}_A)^{-1/2} \overline{\mathbf{V}} \quad , \quad (21)$$

where  $\overline{\mathbf{V}}$  can be obtained by applying singular value decomposition (SVD) in the following matrix;

$$\sum^{1/2} \mathbf{V}^H \mathbf{F}_A (\mathbf{F}_A^H \mathbf{F}_A)^{-1/2} = \overline{\mathbf{U}} \sum^{1/2} \overline{\mathbf{V}}^H \quad , \quad (22)$$

$$\mathbf{H} = \mathbf{U} \sum^{1/2} \mathbf{V}^H \quad . \quad (23)$$

Then the spectral efficiency of the corresponding mmWave channel can be expressed by,

$$S(\gamma) = \mathbb{E} \left[ \log \det \left( \mathbf{I}_{N_R} + \frac{\mathbf{H} \mathbf{F}_A \mathbf{F}_D \mathbf{F}_D^H \mathbf{F}_A^H \mathbf{H}^H}{N_{RF} \gamma} \right) \right] \quad , \quad (24)$$

where  $\mathbf{I}_{N_R}$  is an  $N_R \times N_R$  identity matrix,  $\gamma$  denotes the signal to noise ratio (SNR).

Here we further defining the objective function in (5) as,

$$\theta_{\text{obj}} = (\beta_{ca} p_{ca} + \beta_{st} p_{st}) p_{in} \quad , \quad (25)$$

where  $p_{ca}$  is the spectral efficiency, and  $p_{st}$  is the predicted duration that the beamforming gain of the moving vehicle can stay beyond a given threshold  $\gamma_{st}$  with the current beamforming pattern. In this paper, the values of  $p_{ca}$  and  $p_{st}$  are the only feedback information required to operate ASA.

As the spectral efficiency optimized baseband precoding method for a given analog precoder is expressed in (20), the upper bound of, i.e.,  $\theta_{\text{max}}$  in (13) is further expressed as,

$$\theta_{\text{max}} = (\beta_{ca} p_{ca}^* + \beta_{st} p_{st}^*) p_{in} \quad , \quad (26)$$

where  $p_{ca}^*$  is the spectral efficiency with the spectral efficiency optimized hybrid precoding method expressed in (20), and  $p_{st}^*$  is the upper bound of the predicted duration that beamforming gain of the moving vehicle can stay beyond a given threshold  $\gamma_{st}$  with the current beamforming pattern. The value of  $p_{ca}^*$  is the only information that is needed to do the ASA-assisted uplink beamforming, and this information can be achieved easily by the RSI and feedback to the vehicle. Thus, with this approach, the uplink beamforming can be done without channel state information which is very hard to achieve in mmWave based V2I communications.

As the hybrid precoding method in (20) is based on full perfect knowledge of the channel state information (CSI), here we assume full channel information can be achieved by

perfect channel estimation, i. e., the transmitter can achieve the path gain of each propagation path. Then, based on (24), if the  $m_{rf}$  ( $m_{rf} \leq N_{RF}$ ) RF chains with the strongest average path gain are chosen to do the hybrid precoding, the corresponding analog precoder can be constructed as,

$$\begin{aligned} \mathbf{F}_A^* &= [\mathbf{a}_T(\varphi_1) \dots \mathbf{a}_T(\varphi_{m_{rf}})] \\ &= \mathbf{A}_T [1, \dots, N_{m_{rf}}] \end{aligned} \quad (27)$$

In other words, by configuring the above analog precoder, uplink analog beamforming can be achieved with the  $m_{rf}$  strongest propagation paths. Under these conditions, the spectral efficiency corresponding to this precoding method will be higher compared with the proposed codebook based hybrid precoding described in section 3, part A, i. e.,  $SE^* \geq SE$  with (28) and (29),

$$SE^* = \mathbb{E} \left[ \log \det (\mathbf{I}_{N_R} + \frac{\gamma}{m_{rf}} \mathbf{H} \mathbf{F}_A^* \mathbf{F}_D^* (\mathbf{F}_D^*)^H (\mathbf{F}_A^*)^H \mathbf{H}^H) \right], \quad (28)$$

$$SE = \mathbb{E} \left[ \log \det (\mathbf{I}_{N_R} + \frac{\gamma}{m_{rf}} \mathbf{H} \mathbf{F}_H^{\{s,k,m\}} (\mathbf{F}_H^{\{s,k,m\}})^H \mathbf{H}^H) \right], \quad (29)$$

where  $SE^* = p_{ca}^*$  is the spectral efficiency with  $m_{rf}$  activated RF chains, which uses RF chains to do beamforming through the  $m_{rf}$  strongest propagation paths.  $SE = p_{ca}$  is the spectral efficiency of the proposed codebook based hybrid precoding method, with the codeword located on position  $\{s, k, m\}$  of the codebook. Notice that the values of  $p_{ca}$  and  $p_{st}$  are the only information needed to do the ASA-assisted uplink beamforming and this information can be achieved easily by the RSI and feedback to the vehicle. Thus, with this approach, uplink beamforming can be done without channel state information, which is very difficult to achieve in mmWave based V2I communications. The cause of the performance gap between these two precoding methods is channel information. For instance, using the full channel information, the optimized digital precoder can be constructed as,

$$\mathbf{F}_D^* = \left( (\mathbf{F}_A^*)^H \mathbf{F}_A^* \right)^{-1/2} \bar{\mathbf{V}}, \quad (30)$$

where,  $\bar{\mathbf{V}}$  is acquired by singular value decomposition (SVD) as,

$$\mathbf{H} = \mathbf{U} \Sigma^{1/2} \mathbf{V}^H, \quad (31)$$

$$\Sigma^{1/2} \mathbf{V}^H \mathbf{F}_A^* \left( (\mathbf{F}_A^*)^H \mathbf{F}_A^* \right)^{-1/2} = \bar{\mathbf{U}} \Sigma^{1/2} (\bar{\mathbf{V}})^H. \quad (32)$$

Based on the analysis in [42], when signal to noise ratio (SNR) is high enough, (28) can be further derived as,

$$SE^* = \mathbb{E} \left[ \log \det (\mathbf{I}_{N_R} + \frac{\gamma}{m} \mathbf{H} \mathbf{F}_A^* \mathbf{F}_D^* (\mathbf{F}_D^*)^H (\mathbf{F}_A^*)^H \mathbf{H}^H) \right]. \quad (33)$$

Moreover, (33) can be further approximated as (34) [42],

$$SE^* \approx \sum_{i=1}^{m_{rf}} \exp \left( \frac{1}{r_i \rho} \right) E_1 \left( \frac{1}{r_i \rho} \right) + L \sum_{k=1}^4 \sum_{e=0}^k \frac{(-1)^{e+1}}{k} \binom{k}{e} \mu_e^A, \quad (34)$$

Notice that the channel state information-based beamforming method is only used to better explain the derivation process of (34), which is an approximation of (33), based on stochastic analysis. Also, as can be observed, the computation of (34) does not need the channel state information. More specifically, the proposed ASA-assisted uplink beamforming method does not require full channel estimation and therefore, has much lower complexity compared with the channel estimation-based beamforming method. In fact, the only feedback information that it needs is the quality of the current link (i.e.,  $p_{ca}$  and  $p_{st}$ ). Such information can be easily transmitted to vehicles, which we refer to as a ‘‘limited feedback’’ information.

In (34),  $E_1$  and other parameters are expressed as,

$$E_1 \left( \frac{1}{r_i \rho} \right) = \int_{\frac{1}{r_i \rho}}^{\infty} t^{-1} \exp(-t) dt, \quad (35)$$

and,

$$\left\{ \begin{array}{l} \mu_1^A = 1 \\ \mu_2^A = 1 + \frac{L-1}{N_R} \\ \mu_3^A = 1 - \frac{3}{N_R} + \frac{2}{N_R^2} + \left( 1 - \frac{1}{N_R} \right) \frac{3L}{N_R} + \left( \frac{L}{N_R} \right)^2 \\ \mu_4^A = 1 - \frac{20}{3N_R} + \frac{12}{N_R^2} - \frac{19}{3N_R^3} + \left( \frac{20}{3} - \frac{18}{N_R} + \frac{34}{3N_R^2} \right) \left( \frac{L}{N_R} \right) + 6 \left( 1 - \frac{1}{N_R} \right) \left( \frac{L}{N_R} \right)^2 + \left( \frac{L}{N_R} \right)^3 \end{array} \right. \quad (36)$$

Where  $L$  is the number of the propagation paths,  $r_i$  is the large scale fading of the corresponding propagation path, and  $\rho = \frac{N_T N_R}{m_{rf}} \gamma$ .

Then, the upper bound of the spectral efficiency of the proposed codebook-based hybrid precoding method can be achieved by using(34)(35), and (36) together.

Defining  $p_{st}$  as the duration that a moving vehicle can stay in the main lobe of the beamforming pattern, based on [43], the shape of the main lobe of a beam can be considered as a sector. Let us define a function  $f_t(x)$  as  $f_t(x) = \exp \left( j \frac{2\pi}{\lambda_w} k d_A \sin(x) \right)$  for further analysis. Thus, by  $\Theta_{ML}^{\{s,k,m\}}$  being the width of the main lobe of the beam pattern:  $\mathbf{F}_H^{\{s,k,m\}}$ , in the angular domain,  $\Theta_{ML}^{\{s,k,m\}}$  can be achieved by solving the following equations;

$$\frac{\sum_{k=0}^{N_T-1} \mathbf{F}_H^{\{s,k,m\}} f_t \left( \theta_{ML}^{\{s,k,m\}} \right)}{\sum_{k=0}^{N_T-1} \mathbf{F}_H^{\{s,k,m\}} f_t \left( \frac{2\pi}{M^{s-1}} (k-1) + m-1 \right)} = \gamma_{ang}. \quad (37)$$

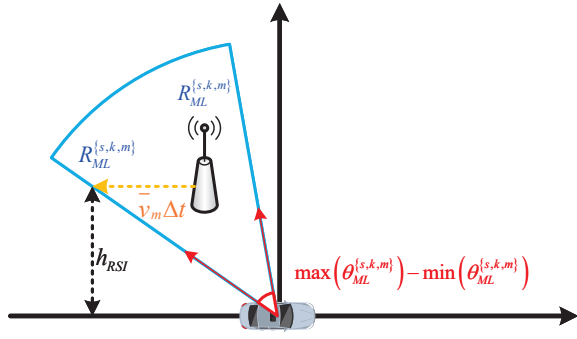


Fig. 4. How to achieve the value of  $p_{st}^*$ .

$$\Theta_{ML}^{\{s,k,m\}} = \max(\theta_{ML}^{\{s,k,m\}}) - \min(\theta_{ML}^{\{s,k,m\}}) \quad , \quad (38)$$

where,  $\gamma_{ang}$  is a given threshold of the decreasing ratio of beamforming gain. Let us set the radius of the sector of beam pattern  $\mathbf{F}_H^{\{s,k,m\}}$  as  $R_{ML}^{\{s,k,m\}}$ , and define  $R_{ML}^{\{s,k,m\}}$  as the maximum distance between the vehicle and the associated RSI to keep the value of large scale fading larger than a given threshold  $\gamma_{pl}^{\{s,k,m\}}$ . Then  $R_{ML}^{\{s,k,m\}}$  is expressed as:  $R_{ML}^{\{s,k,m\}} = \alpha_p \sqrt{1/\gamma_{pl}^{\{s,k,m\}}}$ , where  $\alpha_p$  is the path loss exponent.

Thus, the upper bound of  $p_{st}$  among all the beamforming patterns can be obtained by solving the following problem;

$$\begin{aligned} p_{st}^* &= \max \sqrt{(R_b \cos \theta_b - R_e \cos \theta_e)^2 / \bar{v}_m} \\ \text{subject to } & h_{RSI} \leq R_b, R_e \\ & R_b, R_e \leq R_{ML}^{\{s,k,m\}} \\ & R_b \sin \theta_b = R_e \sin \theta_e = h_{RSI} \\ & \min(\theta_{ML}^{\{s,k,m\}}) \leq \theta_b, \theta_e \\ & \theta_b, \theta_e \leq \max(\theta_{ML}^{\{s,k,m\}}) \quad . \end{aligned} \quad (39)$$

In (39),  $p_{st}^*$  is further expressed as,

$$p_{st}^* = 2 \sqrt{\left(R_{ML}^{\{1, \cdot, \cdot\}}\right)^2 - h_{RSI}^2} \quad . \quad (40)$$

Thus, the  $\theta_{\max}$  can be computed by using,

$$\begin{aligned} \theta_{\max} &= \left( \beta_{ca} \left( \sum_{i=1}^{m_{rf}} \exp\left(\frac{1}{r_i \rho}\right) E_1\left(\frac{1}{r_i \rho}\right) \right) \right. \\ &+ L \sum_{k=1}^4 \sum_{e=0}^k \frac{(-1)^{e+1}}{k} \binom{k}{e} \mu_e^{\mathbf{A}} \left. \right) + \\ &2 \beta_{st} \sqrt{\left(R_{ML}^{\{1, \cdot, \cdot\}}\right)^2 - h_{RSI}^2} p_{in} \quad , \end{aligned} \quad (41)$$

with (35) and (36).

#### IV. SIMULATION RESULTS

The values of the default parameters are set as shown in Table I.

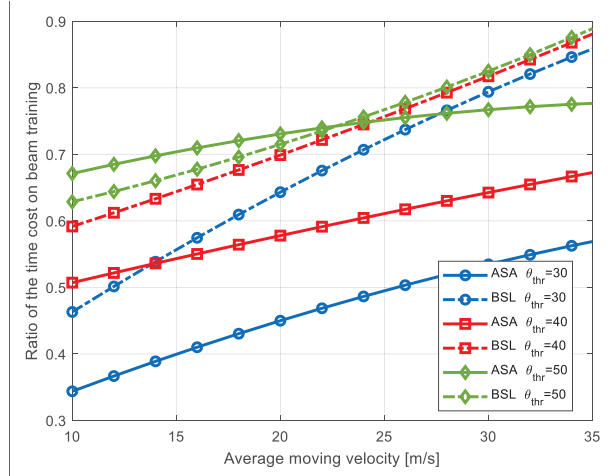


Fig. 5. Ratio of the time cost in beam training with respect to different beam training methods and different  $\theta_{thr}$ .

We assume that there is only one vehicle in the lane and its movement is governed by a Gauss-Markov mobility model. In each time slot, the uplink beamforming is driven by ASA while the vehicle is moving. In our experiments, we get the total time slots;  $N_{\Delta t}$ , which is used for beam training. By denoting the total time slots of simulation as  $N_{sim}$ , the ratio of the time cost in beam training can be expressed as  $\varpi = N_{\Delta t}/N_{sim}$ . The simulation results of ASA are compared with the beam training method used in IEEE 802.11ad [20], which is based on complicated channel estimation that requires full channel state information. The IEEE 802.11ad based simulation results will be displayed with the label BSL in the following figures.

Fig. 5 shows the ratio of the time cost on beam training  $\varpi$  with respect to different  $\theta_{thr}$  and beamforming methods. As we can see from this figure,  $\varpi$  increases as the average velocity increases. On the other hand,  $\varpi$  also increases at a higher  $\theta_{thr}$ . This is mainly due to the fact that when the vehicle velocity or  $\theta_{thr}$  is very large, which causes the link quality to become highly fluctuant, the link can only remain stable for a short period of time. Thus, the vehicle may spend more time searching for acceptable beamforming patterns. When  $\theta_{thr}$  is small, e. g.,  $\theta_{thr} = 30$  or  $\theta_{thr} = 40$ , the performance of ASA can improve substantially compared with the baseline method (i.e., BSL). This is mainly because when  $\theta_{thr}$  is small, more beamforming patterns in the codebook can be used to do uplink beamforming. As the result, ASA consumes very little time to determine the beamforming patterns, and once it is selected, the ASA will retain the beamforming pattern until it becomes unacceptable. Because when the beamforming pattern is acceptable, the value of  $\alpha$  will be very large so that the  $P_i$  (i.e., the probability to be selected as the beamforming pattern) of current beamforming pattern will be much larger than other candidates. At the same time, when  $\theta_{thr}$  is large (like average velocity),

TABLE I  
VALUES OF SYMBOLS USED IN SIMULATION

Symbol	Definition/explanation	Value
$\lambda_{RSI}$	Density of RSIs	0.02
$L_R$	Length of the road	2000 m
$h_{RSI}$	Distance between RSIs and the road	20 m
$\theta_{thr}$	The threshold of the value of the objective function	40
$\alpha_p$	Path loss exponent	4.5
$N_A$	Maximum resolution of the codebook	128
$N_{RF}$	Number of RF chains	16
$N_T$	Number of transmit antennas	64
$N_{can}$	Number of candidate analog beamforming codeword	64
$N_R$	Number of receive antennas	16
$M_{co}$	Number of codewords in the codebook	256
$\gamma$	Signal to noise ratio	100
$v_s$	Parameter of ASA	50
$k_s$	Parameter of ASA	5
$\beta_{ca}$	Parameter of ASA	0.3
$\beta_{st}$	Parameter of ASA	0.7

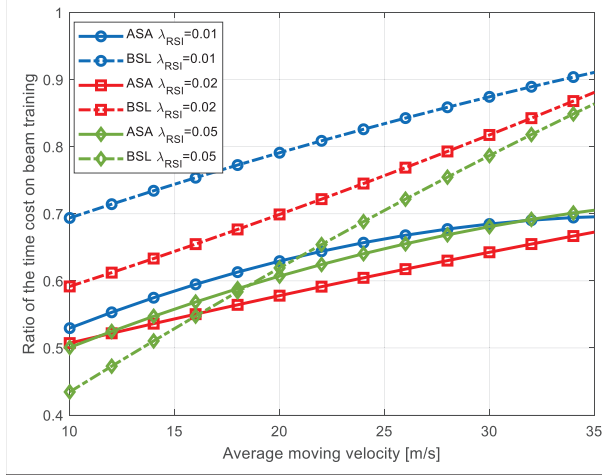


Fig. 6. Ratio of the time cost on beam training with respect to different beam training methods and different  $\lambda_{RSI}$ .

it takes more time for ASA to find a suitable beamforming pattern from the codebook. Under these conditions, since the channel condition is not fluctuant when the moving velocity is small, the performance of baseline method becomes better than ASA. More specifically, when  $\theta_{thr}$  is large and the average moving velocity is also large, the performance of ASA becomes far better than the baseline method, which is due to deteriorated channel conditions.

Fig. 6 shows the ratio of the time cost on beam training  $\varpi$  with respect to a different RSI density;  $\lambda_{RSI}$ , and a beamforming method. As shown in the figure,  $\varpi$  increases with increasing average velocity. On the other hand,  $\varpi$  decreases at a higher  $\lambda_{RSI}$ , but when  $\lambda_{RSI}$  is generally small (e. g.,  $\lambda_{RSI} = 0.01$  or  $\lambda_{RSI} = 0.02$ ). Nonetheless, when  $\lambda_{RSI}$  is as large as  $\lambda_{RSI} = 0.05$ , the  $\varpi$  becomes larger compared with  $\lambda_{RSI} = 0.01$  or  $\lambda_{RSI} = 0.02$ . Also, when  $\lambda_{RSI}$  is small, the performance of ASA is far better than that of the baseline method. These results also indicate

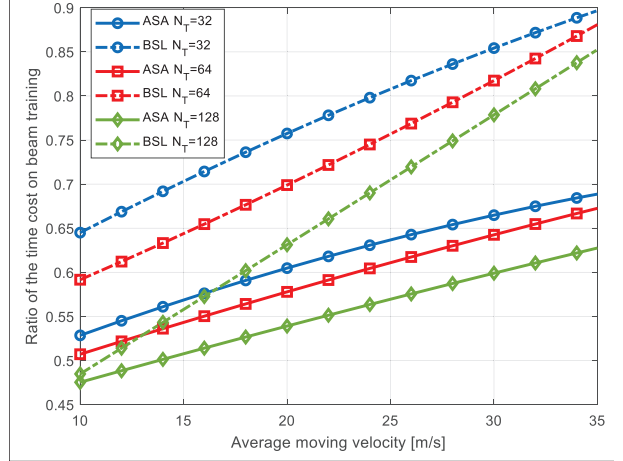


Fig. 7. Ratio of the time cost on beam training with respect to different beam training methods and different  $N_T$ .

that the beamforming pattern with a narrower beam is better for uplink beamforming when  $\lambda_{RSI}$  is large and the moving velocity of the vehicle is small.

Fig. 7 shows the ratio of the time cost on beam training  $\varpi$  with respect to different numbers of transmit antennas;  $N_T$ . As can be seen,  $\varpi$  increases at higher average velocities, and decreases with a higher number of antennas. This is because the number of transmit antennas has a strong effect on channel capacity, hence the time consumed by ASA to search for an acceptable beamforming pattern becomes smaller at a higher number of antennas;  $N_T$ . Also, the performance of ASA becomes much better than that of the baseline method when the value of  $N_T$  is changing.

Fig. 8 shows the spectral efficiency with respect to a different RSI density;  $\lambda_{RSI}$ , and a beamforming method. As we can see from this figure, the spectral efficiency decreases with the increase of the average velocity. The spectral efficiency of ASA is worse than baseline method

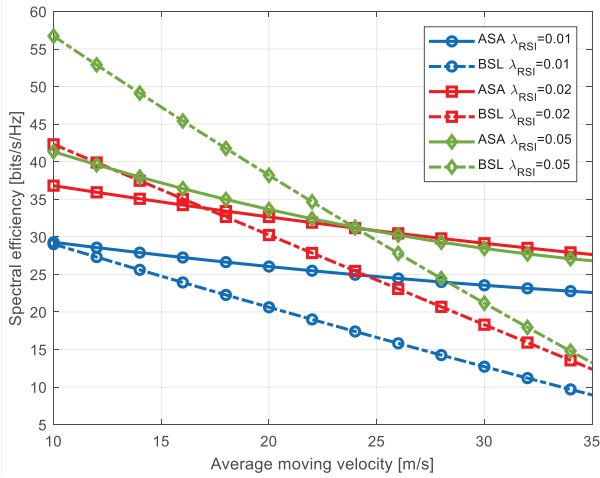


Fig. 8. Spectral efficiency with respect to different beam training methods and different  $\lambda_{RSI}$ .

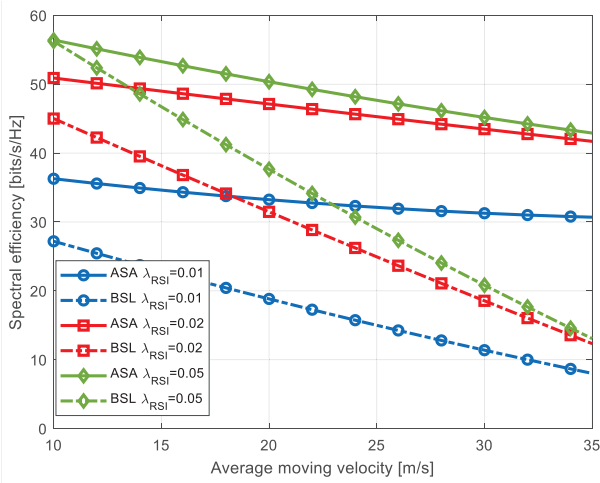


Fig. 9. Spectral efficiency with respect to different beam training methods and different  $\lambda_{RSI}$ , assuming the vehicles have unlimited computing ability.

with lower velocity, and better than the baseline method when the average velocity is high. This is because when the velocity is low, the baseline method with a narrower beam and higher transmission rate compared with ASA is more spectral efficient. On the other hand, when average velocity is high, the ASA with self-adaptive beamforming pattern has a better performance than the baseline method. Moreover, the spectral efficiency of the baseline method increases with the increase of  $\lambda_{RSI}$ . However, the spectral efficiency of ASA with  $\lambda_{RSI} = 0.02$  is higher than the spectral efficiency with  $\lambda_{RSI} = 0.05$ . This is because the ratio of the time cost on beam training;  $\varpi$  is higher when  $\lambda_{RSI} = 0.05$  compared with  $\lambda_{RSI} = 0.02$ , as fig.6 shows. This result indicates that the proposed ASA-assisted beamforming method does not require densely deployed RSIs to achieve a good performance.

By assuming that vehicles have unlimited computing ability (i. e., there is no time cost on running training algorithms), Fig. 9 shows the spectral efficiency with respect to a different RSI density;  $\lambda_{RSI}$ , using different beamforming methods. As can be seen, the performance of both baseline algorithms and ASA decrease with the increasing velocity. However, compared with baseline algorithms, the performance of ASA decreases at a much slower pace. On the other hand, the performance of both baseline algorithms and ASA increase at higher RSI densities. These results indicate that for vehicles with more advanced computing ability, the performance of ASA will be far better.

## V. CONCLUSIONS

This paper mainly focuses on uplink beamforming of vehicle to RSI communications. Due to the higher velocity of vehicles compared with pedestrians, the channel conditions of vehicle communication are more fluctuant and less stable. A codebook based biological inspired algorithm named ASA is proposed to enhance the stability and robustness of the communication link when uplink beamforming is considered for communication between vehicles and RSIs. The simulation results verify that the time consumption that is required for beam training becomes highly efficient when ASA is used for fast-moving vehicles. Finally, it is important to point out that unlike the baseline system, which requires the CSI, the proposed ASA-assisted beamforming scheme operates with a very limited channel information.

## VI. APPENDIX

With the above approach, we can construct a codebook to support different beam patterns with different transmitting directions and beam widths to do uplink beamforming for V2I communications.

Defining  $G_a^{\{s,k,m\}} = \left\| \mathbf{F}_H^{\{s,k,m\}} - \mathbf{F}_A^{\{s,k,m\}} \mathbf{F}_D^{\{s,k,m\}} \right\|_F$ , where  $\|\cdot\|_F$  is the Frobinus norm of the corresponding matrix. Consequently, the design of the hybrid analog and digital training precoding matrices is accomplished by solving the following problems [41];

$$\begin{aligned} \left\{ \mathbf{F}_A^{\{s,k,m\}*}, \mathbf{F}_D^{\{s,k,m\}*} \right\} &= \arg \min G_a^{\{s,k,m\}}, \\ \text{subject to } \left[ \mathbf{F}_A^{\{s,k,m\}} \right]_{:,i} &\in \left\{ [\mathbf{A}_{can}]_{:,l} \mid 1 \leq l \leq N_{can} \right\} \\ i &= 1, 2, \dots, N_{RF} \\ (G_a^{\{s,k,m\}})^2 &= 1. \end{aligned} \quad (42)$$

Where  $N_{RF}$  is the number of activated RF chains,  $[\mathbf{A}_{can}]_{:,l}$  is the  $l$ th column of matrix  $\mathbf{A}_{can}$ , and  $\mathbf{A}_{can}$  is a  $N_T \times N_{can}$  candidate analog precoding matrix defined as,

$$[\mathbf{A}_{can}]_{v,w} = \frac{1}{\sqrt{N_T}} j^{Fl[(v-1)Mod[(w-1)+\frac{N_T}{2}, N_T]/(N_T/4)]}, \quad (43)$$

where  $[\cdot]_{v,w}$  represents the entry in the  $v$ th row,  $w$ th column of a matrix with  $1 \leq v \leq N_T$  and  $1 \leq w \leq N_{RF}$ ,  $Fl[\cdot]$  is the function that returns the biggest integer smaller than or equal to its argument, and  $Mod[\cdot, \cdot]$  is the modulo operation.

Thus, given the matrix of possible analog beamforming vectors, the optimization problem in (43) can be further solved as a sparse approximation problem similar to the optimization problem in [31], with the corresponding optimized hybrid precoding matrix as,

$$\mathbf{F}_H^{\{s,k,m\}} = C_s (\mathbf{A}_{BS,D} \mathbf{A}_{BS,D}^H)^{-1} \mathbf{A}_{BS,D} \mathbf{G}^{\{s,k,m\}}, \quad (44)$$

where  $\mathbf{A}_{BS,D}$  is expressed as,

$$\mathbf{A}_{BS,D} = [\mathbf{a}_T(\varphi_1) \dots \mathbf{a}_T(\varphi_{N_A})], \quad (45)$$

with,

$$\mathbf{a}_T(\varphi_u) = \frac{1}{\sqrt{N_T}} \left[ 1, e^{j \frac{2\pi}{\lambda} d \sin(\varphi_u)}, \dots, e^{j \frac{2\pi}{\lambda} d (N_T-1) \sin(\varphi_u)} \right], \quad (46)$$

and,

$$\varphi_u = \frac{2\pi u}{N_A} \quad u = 0, 1, \dots, N_A - 1 \quad . \quad (47)$$

$\mathbf{G}^{\{s,k,m\}}$  is a  $N_A \times 1$  matrix where each column  $m$  containing 1 in the locations  $u$  if  $u \in \mathcal{I}(s, k, m)$ , and zeros in the positions if  $u \notin \mathcal{I}(s, k, m)$ , with,

$$\mathcal{I}(s, k, m) = \left\{ \frac{N_A}{M^s} (M(k-1) + m - 1) + 1, \dots, \dots, \frac{N_A}{M^s} (M(k-1) + m) \right\} \quad (48)$$

By using the algorithm in [42], we can get the hybrid precoding matrix and the corresponding analog and baseband precoding matrix for each position  $\{s, k, m\}$  in the codebook  $\mathcal{F}$ .

## REFERENCES

- [1] Edfors, Ove, and F. Tufvesson, "Massive MIMO for next generation wireless systems," 2015.
- [2] L. Lu, G. Y. Li, A. L. Swindlehurst, A. Ashikhmin and R. Zhang, "An Overview of Massive MIMO: Benefits and Challenges," *IEEE J. Sel. Topics in Signal Processing*, vol. 8, no. 5, pp. 742–758, Oct. 2014.
- [3] J. Hoydis, S. ten Brink and M. Debbah, "Massive MIMO in the UL/DL of Cellular Networks: How Many Antennas Do We Need?," *IEEE Commun. Surveys and Tutorials*, vol. 20, no. 4, pp. 3060–3097, Fourthquarter 2018.
- [4] I. Ahmed et al., "A Survey on Hybrid Beamforming Techniques in 5G: Architecture and System Model Perspectives," *IEEE J. Sel. Areas Commun.*, vol. 31, no. 2, pp. 160–171, Feb. 2013.
- [5] F. Tang, Y. Kawamoto, N. Kato and J. Liu, "Future Intelligent and Secure Vehicular Network Toward 6G: Machine-Learning Approaches," *Proceedings of the IEEE*.
- [6] W. Viriyasitavat, M. Boban, H. Tsai and A. Vasilakos, "Vehicular Communications: Survey and Challenges of Channel and Propagation Models," *IEEE Veh. Tech. Mag.*, vol. 10, no. 2, pp. 55–66, June 2015.
- [7] M. Cudak, T. Kovarik, T. A. Thomas, A. Ghosh, Y. Kishiyama and T. Nakamura, "Experimental mm wave 5G cellular system," *2014 IEEE Globecom Workshops*, Austin, TX, 2014, pp. 377–381.
- [8] A. Ghazal, C. Wang, B. Ai, D. Yuan and H. Haas, "A Nonstationary Wideband MIMO Channel Model for High-Mobility Intelligent Transportation Systems," *IEEE Trans. Intel. Trans. Systems*, vol. 16, no. 2, pp. 885–897, April 2015.
- [9] X. Gao, L. Dai, S. Han, C. I and R. W. Heath, "Energy-Efficient Hybrid Analog and Digital Precoding for MmWave MIMO Systems With Large Antenna Arrays," *IEEE J. Sel. Areas Commun.*, vol. 34, no. 4, pp. 998–1009, April 2016.
- [10] L. Liang, W. Xu and X. Dong, "Low-Complexity Hybrid Precoding in Massive Multiuser MIMO Systems," *IEEE Wireless Commun. Letters*, vol. 3, no. 6, pp. 653–656, Dec. 2014.
- [11] A. Alkhateeb, G. Leus and R. W. Heath, "Limited Feedback Hybrid Precoding for Multi-User Millimeter Wave Systems," *IEEE Trans. Wireless Commun.*, vol. 14, no. 11, pp. 6481–6494, Nov. 2015.
- [12] X. Yu, J. Shen, J. Zhang and K. B. Letaief, "Alternating Minimization Algorithms for Hybrid Precoding in Millimeter Wave MIMO Systems," *IEEE J. Sel. Topics in Signal Processing*, vol. 10, no. 3, pp. 485–500, April 2016.
- [13] J. Zhao, F. Gao, W. Jia, S. Zhang, S. Jin and H. Lin, "Angle Domain Hybrid Precoding and Channel Tracking for Millimeter Wave Massive MIMO Systems," *IEEE Trans. Wireless Commun.*, vol. 16, no. 10, pp. 6868–6880, Oct. 2017.
- [14] S. Park, A. Alkhateeb and R. W. Heath, "Dynamic Subarrays for Hybrid Precoding in Wideband mmWave MIMO Systems," *IEEE Trans. Wireless Commun.*, vol. 16, no. 5, pp. 2907–2920, May 2017.
- [15] C. Rusu, R. Mndez-Rial, N. Gonzalez-Prelcic and R. W. Heath, "Low Complexity Hybrid Precoding Strategies for Millimeter Wave Communication Systems," *IEEE Trans. Wireless Commun.*, vol. 15, no. 12, pp. 8380–8393, Dec. 2016.
- [16] M. R. Castellanos et al., "Channel-Reconstruction-Based Hybrid Precoding for Millimeter-Wave Multi-User MIMO Systems," *IEEE J. Sel. Topics in Signal Processing*, vol. 12, no. 2, pp. 383–398, May 2018.
- [17] A. Yang, Y. Jing, C. Xing, Z. Fei, and J. Kuang, "Performance analysis and location optimization for massive MIMO systems with circularly distributed antennas," *IEEE Trans. Wireless Commun.*, vol. 14, no. 10, pp. 5659–5671, Oct. 2015.
- [18] A. Yang, Z. He, C. Xing, Z. Fei, and J. Kuang, "The role of large-scale fading in uplink massive MIMO systems," *IEEE Trans. Veh. Tech.*, vol. 65, no. 1, pp. 477–483, Jan. 2016.
- [19] S. Gong, C. Xing, Z. Fei, and S. Ma, "Millimeter-wave secrecy beamforming designs for two-way amplify-and-forward MIMO relaying networks," *IEEE Trans. Veh. Tech.*, vol. 66, no. 3, pp. 2059–2071, Mar. 2017.
- [20] M. Giordani, M. Polese, A. Roy, D. Castor and M. Zorzi, "A Tutorial on Beam Management for 3GPP NR at mmWave Frequencies," *IEEE Commun. Surveys and Tutorials*, vol. 21, no. 1, pp. 173–196, Firstquarter 2019.
- [21] Y. Wang, K. Venugopal, A. F. Molisch and R. W. Heath, "MmWave Vehicle-to-Infrastructure Communication: Analysis of Urban Microcellular Networks," *IEEE Trans. Veh. Tech.*, vol. 67, no. 8, pp. 7086–7100, Aug. 2018.
- [22] A. Tassi, M. Egan, R. J. Piechocki and A. Nix, "Modeling and Design of Millimeter-Wave Networks for Highway Vehicular Communication," *IEEE Trans. Veh. Tech.*, vol. 66, no. 12, pp. 10676–10691, Dec. 2017.
- [23] H. Wymeersch, G. Seco-Granados, G. Destino, D. Dardari and F. Tufvesson, "5G mmWave Positioning for Vehicular Networks," *IEEE Wireless Commun.*, vol. 24, no. 6, pp. 80–86, Dec. 2017.
- [24] V. Va, J. Choi, T. Shimizu, G. Bansal and R. W. Heath, "Inverse Multipath Fingerprinting for Millimeter Wave V2I Beam Alignment," *IEEE Trans. Veh. Tech.*, vol. 67, no. 5, pp. 4042–4058, May 2018.
- [25] Z. Zhang, H. Wu, H. Zhang, H. Dai and N. Kato, "Virtual-MIMO-Boosted Information Propagation on Highways," *IEEE Trans. Wireless Commun.*, vol. 15, no. 2, pp. 1420–1431, Feb. 2016.
- [26] C. Ren, J. Chen, Y. Kuo and L. Yang, "Differential successive relaying scheme for fast and reliable data delivery in vehicular ad hoc networks," *IET Commun.*, vol. 9, no. 8, pp. 1088–1095, 21 5 2015.
- [27] A. Alkhateeb and R. W. Heath, "Frequency Selective Hybrid Precoding for Limited Feedback Millimeter Wave Systems," *IEEE Trans. Commun.*, vol. 64, no. 5, pp. 1801–1818, May 2016.
- [28] Z. Xiao, P. Xia and X. Xia, "Channel Estimation and Hybrid Precoding for Millimeter-Wave MIMO Systems: A Low-Complexity Overall Solution," *IEEE Access*, vol. 5, pp. 16100–16110, 2017.

- [29] S. He, J. Wang, Y. Huang, B. Ottersten and W. Hong, "Codebook-Based Hybrid Precoding for Millimeter Wave Multiuser Systems," *IEEE Trans. Signal Processing*, vol. 65, no. 20, pp. 5289–5304, Oct. 2017.
- [30] H. Seleem, A. I. Sulyman and A. Alsanie, "Hybrid Precoding-Beamforming Design With Hadamard RF Codebook for mmWave Large-Scale MIMO Systems," *IEEE Access*, vol. 5, pp. 6813–6823, 2017.
- [31] D. De Donno, J. P. Beltrn, D. Giustiniano and J. Widmer, "Hybrid analog-digital beam training for mmWave systems with low-resolution RF phase shifters," *2016 IEEE International Conference on Communications Workshops (ICC)*, Kuala Lumpur, pp. 700–705, 2016.
- [32] V. Raghavan et al., "Statistical Blockage Modeling and Robustness of Beamforming in Millimeter-Wave Systems," *IEEE Trans. Microwave Theory and Tech.*, vol. 67, no. 7, pp. 3010–3024, July 2019.
- [33] H. Joudeh and B. Clerckx, "Robust Transmission in Downlink Multiuser MISO Systems: A Rate-Splitting Approach," *IEEE Trans. Signal Processing*, vol. 64, no. 23, pp. 6227–6242, 1 Dec. 2016.
- [34] V. Raghavan, J. Cezanne, S. Subramanian, A. Sampath and O. Koyun, "Beamforming Tradeoffs for Initial UE Discovery in Millimeter-Wave MIMO Systems," *IEEE J. Sel. Topics in Signal Processing*, vol. 10, no. 3, pp. 543–559, April 2016.
- [35] Kashiwagi, Akiko, et al. "Adaptive response of a gene network to environmental changes by fitness-induced attractor selection." *PLoS one* 1.1, e49, 2006.
- [36] K. Leibnitz, N. Wakamiya and M. Murata, "WSN17-3: Self-Adaptive Ad-Hoc/Sensor Network Routing with Attractor-Selection," *IEEE Globecom 2006*, San Francisco, CA, pp. 1–5, 2006.
- [37] D. Tian, J. Zhou, Y. Wang, Y. Lu, H. Xia and Z. Yi, "A Dynamic and Self-Adaptive Network Selection Method for Multimode Communications in Heterogeneous Vehicular Telematics," *IEEE Trans. Intel. Trans. Systems*, vol. 16, no. 6, pp. 3033–3049, Dec. 2015.
- [38] D. Tian et al., "From Cellular Decision Making to Adaptive Hand-off in Heterogeneous Wireless Networks," *IEEE Wireless Commun. Letters*, vol. 7, no. 1, pp. 2–5, Feb. 2018.
- [39] K. Leibnitz and M. Murata, "Attractor selection and perturbation for robust networks in fluctuating environments," *IEEE Network*, vol. 24, no. 3, pp. 14–18, May. 2010.
- [40] Bai, Fan, and Ahmed Helmy. "A survey of mobility models." *Wireless Adhoc Networks*. University of Southern California, 2004.
- [41] A. Alkhateeb, O. El Ayach, G. Leus and R. W. Heath, "Channel Estimation and Hybrid Precoding for Millimeter Wave Cellular Systems," *IEEE J. Sel. Topics in Signal Processing*, vol. 8, no. 5, pp. 831–846, Oct. 2014.
- [42] Z. Zheng and H. Gharavi, "Spectral and Energy Efficiencies of Millimeter Wave MIMO With Configurable Hybrid Precoding," *IEEE Trans. Veh. Tech.*, vol. 68, no. 6, pp. 5732–5746, June 2019.
- [43] S. Noh, M. D. Zoltowski and D. J. Love, "Multi-Resolution Codebook and Adaptive Beamforming Sequence Design for Millimeter Wave Beam Alignment," *IEEE Trans. Wireless Commun.*, vol. 16, no. 9, pp. 5689–5701, Sep. 2017.



**Hamid Gharavi** received his Ph.D. degree from Loughborough University, United Kingdom, in 1980. He joined the Visual Communication Research Department at AT&T Bell Laboratories, Holmdel, New Jersey, in 1982. He was then transferred to Bell Communications Research (Bellcore) after the AT&T-Bell divestiture, where he became a consultant on video technology and a Distinguished Member of Research Staff. In 1993, he joined Loughborough University as a

professor and chair of communication engineering. Since September 1998, he has been with the National Institute of Standards and Technology (NIST), U.S. Department of Commerce, Gaithersburg, Maryland. He was a core member of Study Group XV (Specialist Group on Coding for Visual Telephony) of the International Communications Standardization Body CCITT (ITU-T) and a member of the IEEE 2030 standard working group. His research interests include smart grid, wireless multimedia, mobile communications and wireless systems, mobile ad hoc networks, and visual communications. He received the Charles Babbage Premium Award from the Institute of Electronics and Radio Engineering in 1986, and the IEEE CAS Society Darlington Best Paper Award in 1989. He was the recipient of the Washington Academy of Science Distinguished Career in Science Award for 2017. He served as a Distinguished Lecturer of the IEEE Communication Society. He has been a Guest Editor for a number of special issues of the Proceedings of the IEEE, including Smart Grid, Sensor Networks & Applications, Wireless Multimedia Communications, Advanced Automobile Technologies, and Grid Resilience. He was a TPC Co-Chair for IEEE SmartGridComm in 2010 and 2012. He served as a member of the Editorial Board of Proceedings of the IEEE from January 2003 to December 2008. He was Editor-in-Chief of IEEE Transactions on CAS for Video Technology and IEEE Wireless Communications.



**Junliang Ye** received the B.Sc. degree in communication engineering from the China University of Geosciences, Wuhan, China, in 2011. Then he received his Ph.D. degree from Huazhong University of Science and Technology, Wuhan, China, in 2018. Now he is serving as a guest researcher at National Institute of Standards and Technology (NIST), U.S. Department of Commerce, Gaithersburg, Maryland. His research interests include heterogeneous networks, stochastic

geometry, mobility-based access models of cellular networks, millimeter wave communications, and next-generation wireless communication.